Heritage Science

Open Access

Exploration of coating alternatives for the protection of bare steel and brass in scientific-technical artefacts

María Teresa Molina[1*], Barbara Salvadori[2], Emilio Cano[1], Daniel de la Fuente[1] and Blanca Ramírez-Barat[1]

Abstract

The development of new alternatives for the protection of metallic heritage aims to improve the performance of the coatings used in recent decades. For this purpose, the performance of three novel or poorly explored coatings in this field of study has been evaluated: Owatrol Oil, TiO_2-modified Paraloid B-72 and a hybrid of poly(2-ethyl-2-oxazoline), PEOX and poly(4-hydroxy styrene), PHS as a self-healing coating. These have been compared with coatings widely used in conservation such as: Paraloid B-72, Incralac and microcrystalline wax C80. The coatings were evaluated after accelerated ageing in terms of aesthetic changes (visual observation under stereomicroscope and colour measurements), protective ability (electrochemical impedance spectroscopy) and chemical stability (FTIR). After 500 h of exposure to Xenon-arc lamp, it was observed how the addition of TiO_2 to Paraloid B-72 partially reduces photo-oxidation of the polymer, but at the same time harms the protective ability due to the appearance of defects. The self-healing coating is quite stable and can also regenerates superficial scratches of about 100 µm if subjected to 90% RH. On the other side, Owatrol demonstrated a very poor performance. These advantages and disadvantages in their use have been compared with those of B-72, Incralac and C80 microcrystalline wax, identifying in which cases their application for protection on scientific-technical artefacts may be feasible.

Keywords Scientific-technical heritage, Bare metal, Coatings, Owatrol oil, TiO_2, Self-healing

Introduction

The search for new solutions for the protection of cultural heritage metals against corrosion is a major challenge today. Traditional conservation coatings such as waxes and acrylic resins tend to photo-oxidise [1, 2] and in some cases contain benzotriazole (BTA), having suspected toxicity [3]. In the last decades, alternatives to the most usual coatings used by conservators have been investigated. In addition to their protective capabilities, improvement of other properties of the coatings are sought, trying to improve their performance in specific environments or for specific types of artefacts or surface characteristics [4]. For instance, fluoropolymers have demonstrated to be more chemically inert and stable in outdoor environment [5, 6], and silane-based coatings have improved hydrophobicity [7] or penetration of the coating into the corroded metal [8, 9].

In this direction, efforts have been dedicated in the last years to research on smart coatings, that is, coatings that are capable to react and adapt to external stimuli. Coatings with self-cleaning or superhydrophobic properties are making progress in industrial sectors [10], and their application in heritage is beginning to be explored. This type of coatings has been investigated with the use of oxide nanoparticles mainly in the field of conservation of architectural heritage [11, 12]. These include the use

*Correspondence:
María Teresa Molina
mt.molina@cenim.csic.es
[1] National Centre for Metallurgical Research (CENIM), Spanish National Research Council (CSIC), Avenida Gregorio del Amo, 8, 28040 Madrid, Spain
[2] Institute of Heritage Science (ISPC), National Research Council (CNR), Via Madonna Del Piano 10, 50019 Sesto Fiorentino, Italy

Molina *et al. Heritage Science* (2023) 11:208

Page 2 of 15

of SiO_2 and TiO_2 as photocatalysts capable of creating a surface with nonwetting and self-cleaning properties, and even of decomposing pollutants [13]. The use of these nanoparticles on metals is very limited, but their addition to acrylic or organosilane coatings has started to be investigated [14–17]. TiO_2 stands out as the additive with the most attractive performance, as its photocatalytic activity can improve the polymer's resistance to UV radiation [14, 18]—one of the main degradation agents of commonly used acrylic resins—, while providing self-cleaning and de-polluting abilities. However, at the same time, degradation of the polymer can be induced due to an excess of free radicals [19, 20]. It is therefore necessary to evaluate the pros and cons of use in metal protection and how it can influence the protective ability of the coating.

On the other hand, the application of self-healing coatings has attracted a lot of interest for industrial applications. Their use on metals implies the regeneration of local physical damage caused by external factors that can initiate the corrosion process [21], but their application options on heritage is very limited due to the fact that most of them do not fulfil conservation ethic criteria. A recent work proposes a transparent self-healing coating, easy to synthesise and with promising results, tested on glass slides, which could be suitable for conservation of cultural heritage [22]. It is based on a hybrid polymer of poly(2-ethyl-2-oxazoline), PEOX, and poly(4-hydroxy styrene), PHS, capable of regenerating in high and low humidity, especially when $CaCl_2$ is added. Its main component PEOX is better known as Aquazol©, and it has already been used as a consolidant in stone heritage [23] and as a binder in canvas paintings [24] with satisfactory results.

This research aims to explore the applicability of these alternative coatings for metallic scientific-technical artefacts. This type of heritage have some peculiarities: it includes objects of very different sizes, museographic exhibition requirements, and material compositions, making difficult to achieve optimal conservation conditions [25]. In contrast with archaeological or artistic metallic heritage, which usually have a thick patina or corrosion crust, metallic surfaces in scientific-technical artefacts generally have a "clean", and bare finish that favoured their functioning and use. This finish is usually maintained by conservators depending on the type of object [26, 27] and avoiding damage to original wear

marks or other finishes such as original shellac coatings [1, 28]. Finally, in some cases, artefacts are in operation [29, 30], so the coating may suffer from mechanical damages.

Considering these peculiarities, coatings exhibiting promising features from the literature, such as Paraloid B-72 modified with TiO_2 nanoparticles and the above-mentioned self-healing coating [22], were selected to be evaluated as protective coatings for metals in scientific-technical heritage. Additionally, Owatrol oil is also included as a protective coating in this study. Owatrol is distributed as an "oil-based rust inhibitor" that has being used by conservators in industrial heritage protection exposed to outdoor environments [31]. To the best of our knowledge, only few references report its performance [32–34], but none of them on clean metal surfaces. Therefore, further investigation is needed to determine its protective ability and chemical stability upon ageing, and whether it could also be used on bare metals. These coatings are compared in performance with previously studied and traditionally used such as Paraloid B-72 acrylic resin and C80 microcrystalline wax as coatings with acceptable performance [1, 35] and Incralac, an acrylic resin with corrosion inhibitor widely used in conservation that has demonstrated good protective ability [36–38].

For this work, bare steel and brass have been selected as the most representative metal substrates for scientific-technical collections exposed indoors according to a previous work by the authors [1]. This study will allow complementary comparisons between the coatings already evaluated in the previous reference on these metals using different accelerated ageing conditions, as well as studying the feasibility of applying the alternative coatings according to the additional needs of this type of artefacts.

Materials and methods
Substrate preparation
Brass (CDA 260 alloy) and low carbon steel (Table 1) were selected as substrates for the application of the different coating systems. C and S were determined by infrared absorption method after combustion and the remaining elements by glow-discharge optical emission spectroscopy (GDOES). $5 \times 5 \times 0.2$ cm^3 steel and $5 \times 5 \times 0.03$ cm^3 brass coupons were cut and sanded with P320 and P600 grit emery paper and cleaned with ethanol in an ultrasonic bath in order to degrease and prepare the surface before applying the coatings. Although

Table 1 Elemental composition (mass %) $\pm$ SD of the steel coupons

C	Si	Mn	P	S	Cr	Ni	Al	Cu	Fe
0.026 ± 0.001	< 0.03	0.15	0.014 ± 0.001	0.026 ± 0.0003	0.019 ± 0.001	0.019 ± 0.001	0.036 ± 0.001	0.038 ± 0.001	Balance

Molina *et al. Heritage Science* (2023) 11:208

Page 3 of 15

some scientific-technical artefacts may have some stable oxide layer inside the museum, for this first test exploration with alternative coatings, the metal is lightly sanded to obtain a reproducible and comparable surface and methodology.

Coatings preparation and application

Selected coatings, their composition, code used in this paper and supplier are described in Table 2. Paraloid B-72 was dissolved at 10 wt.% in xylene, C80 microcrystalline was warm dissolved at 80 °C in 10 wt.% white spirit. The application methodology for these coatings was the same as the previous work [39]. For Paraloid B-72 and C80 microcrystalline wax, two layers were applied by brush, with a drying time of 1 week between layers, at room temperature (over 21 °C and 45% RH). Incralac and Owatrol Oil were used as supplied and applied in only one layer. All coatings were left to dry for 2 weeks before testing. This promotes the formation of a dry sufficiently stable layer, i.e., retained solvent does not impair the protective ability of the layer prior to ageing [39].

For the $B72/TiO_2$, nanoparticles with an average diameter of 25 nm in anatase crystalline phase were chosen ($\geq$ 99.5% trace metals basis; REF: 718467, Sigma-Aldrich), as they are more photoactive than other phases such as rutile [18]. To limit the undesirable aesthetic effects due to the white colour of the TiO_2 particles, they were dispersed at low concentration in the acrylic resin (0.5 wt. % in Paraloid B-72). The dispersion was carried out with a magnetic stirrer for 3 h at a temperature of 30 °C and finally ultrasonicated for 15 min before application. The same application methodology was followed as for the acrylic resin without additives.

Hybrids of PEOX (M_w~200,000; REF: 372854, Sigma-Aldrich) and PHS (M_w~11,000; REF: 436216, Sigma-Aldrich) were manufactured by dissolving them in DMF ($\geq$ 99% purity; REF: D158550, Sigma-Aldrich)

at a concentration of 15 wt. % and with a ratio of 70% PEOX/30% PHS. According to [22], the addition of soluble salts such as $CaCl_2$ accelerates the self-healing of the film, however this can lead to corrosion on our surfaces. Still a quick test was made by adding the lowest amount used in that paper: molar ratio of 1:6 according to (Ca^{2+}: carbonyl groups of PEOX) [22]. The resulting PHS/PEOX coatings with and without $CaCl_2$ were applied by brush and left to dry for 48 h in an oven at 60 °C to accelerate the evaporation of the DMF and then left two further weeks before accelerated ageing, as the other coatings.

Artificial ageing

To evaluate the long-term performance of the coatings, they were subjected to photochemical ageing using a SolarBox CO.FO.ME.GRA model 3000e equipped with a Xenon-arc lamp and an outdoor type UV filter with cut-off < 290 nm to eliminate radiation not present in the external sunlight. According to ISO 16474–2:2014 [40], the irradiance was maintained at 500 W/m^2 and the black standard temperature (BST) at 60 ± 1 °C. Coupons were studied before (t = 0) and after accelerated UV exposure for 500 h (t = 1). Inside a museum the radiation would not be as aggressive but for this study it is intended to evaluate the photocatalytic action of TiO_2 since at λ > 390 nm it could be limited [41] as well as to know if all coatings perform well under severe conditions.

Characterisation techniques

Thickness measurements were taken before and after ageing with an Elcometer 456, using a probe for ferrous and non-ferrous materials based on electromagnetic induction. A 12.3-micron gauge (Ser. Nº KC8913) was used for instrument calibration and a thicker 23.9-micron gauge (Ser. Nº KC8888) was used to interpose between the probe and the C80 coating to avoid pressure marks,

Table 2 Tested coatings

Coating	Composition	Code	Supplier
Paraloid B-72	Methyl acrylate and ethyl methacrylate	B72	Kremer Pigmente GmbH & Co
Microcristalina C80	Microcrystalline wax + other waxes may be added*	C80	C.T.S España S.L
Incralac	Ethyl acrylate and methyl methacrylate (Paraloid B-44) + Benzotriazole (BTA) + plasticising agents	INC	Kremer Pigmente GmbH & Co
Owatrol oil	Alkyd-based resin resin from vegetable oils (No information on possible additives)	OW	AGARAGAR Quinta y Galán, S.L
Paraloid B-72 and TiO_2 nanocomposite	B72 + Titanium(IV) oxide; P25 nanoparticles (NPs)	B72/TiO_2	Merck KGaA—Sigma-Aldrich Spain
PHS and PEOX blend	Poly(2-ethyl-2-oxazoline) (PEOX) + poly(4-hydroxy styrene) (PHS)	PHS/PEOX	Merck KGaA—Sigma-Aldrich Spain

* C80 is distributed as Cosmolloid H80 but according to its safety data sheet, it may contain a mixture of other waxes

Molina *et al. Heritage Science* (2023) 11:208

Page 4 of 15

which was then subtracted. For each coupon, 16 measurements were taken and then averaged.

For a visual and generalized analysis of the coatings after ageing, macro-scale imaging was obtained with a Canon EOS 7D camera and EF-S 60 mm f/2.8 macro lens. To analyse the defects undergone at a smaller scale, an Olympus BX41M LED reflected light metallurgical microscope with a 10×objective was used. In particular, the defects produced in the TiO$_2$-modified B72 coatings on the two metals were also analysed at the nanoscale with a JEOL JSM 6500F SEM equipped with EBSD. The beam application energy was 14 kV or 7 kV depending on the magnification; 250× or 4000× respectively.

Colour measurements were made with a Konica-Minolta CM-700-d spectrophotometer using the 1976 CIELAB colour space. The standard illuminant was D65 and the observer was set to 10° according to UNE-EN 15886:2010 [42]. The colour coordinates L*, a* and b* were recorded in four zones for each coupon (∅=6 mm) at t=0 and t=1, excluding the specular component (SCE). The instrument was calibrated against a SPEC-TRALON reference before each set of measurements. Since the coupons are made in triplicate, an average is taken for each coating to obtain the L*a*b* values. The colour differences were calculated from the following Eq. (1):

$$\Delta E = \sqrt{(\Delta L^*)^2 + (\Delta a^*)^2 + (\Delta b^*)^2} \qquad (1)$$

Chemical changes of the coatings were evaluated by FTIR in total reflection mode (TR-FTIR). A Bruker Alpha II spectrometer with external reflection module was used and spectra were acquired with a resolution of 4 cm^{-1} in the range 7000–400 cm^{-1}, collecting 64 scans in each area with a spot size of 5 mm. Background was performed on gold plate and data were processed with OPUS 8.7 software. Spectra were represented using the pseudo absorbance [A'=log(1/R); R=reflectance] as the intensity unit. The resulting spectra were comparable with those taken in transmission and ATR. The ATR module was also used with the same spectrometer to analyse the microcrystalline wax C80 with the same measurement conditions as the external reflection module. This will be detailed in Sect. "TR-FTIR measurements".

The spatial distribution of the two-component PHS/PEOX coating was monitored with a Bruker LUMOS II FTIR microscope (Bruker Optics GmbH, Ettlingen, Germany), equipped with a liquid-N$_2$ cooled 32×32 element Focal Plane Array (FPA) detector. FPA-FTIR images were acquired in reflection mode within a 4000–750 cm^{-1} spectral region, as a single FTIR image covering a sampling area of ca. 150×150 mm^2, with resolution 4 cm^{-1} and 128 scans. A single spectrum in each FTIR image represented molecular information acquired from ca. 5×5 μm^2 area on the sample plane. The collected FTIR spectra were processed using OPUS 8.7 software.

Protective properties of the coatings were evaluated by electrochemical impedance spectroscopy (EIS) using the G-PE cell previously developed by the authors for electrochemical analysis in cultural heritage [43, 44]. AISI 316 stainless steel wire (1.5 mm thick) and AISI 316 stainless steel mesh were used as pseudo-reference electrode and counter-electrode, respectively. Distilled water with 10 ppm acetic acid−conductivity of 26.13 μS and pH=6−was used as electrolyte, since this acid is one of the most common pollutants in museum indoors [45]. The solution was gelled with 2 wt. % agarose according to [46] and exposed to an area of 3.14 cm^2 of the working electrode. Spectra were acquired with a Gamry Reference 600 potentiostat, with 20 mV RMS amplitude (at open circuit potential, OCP) and 10 points/decade from 100 kHz to 10 mHz. The system was allowed to stabilise at OCP for 30 min before measurements.

Results and discussion
Aesthetic changes
Visual appearance
Monitoring the visual appearance of coatings after application and accelerated ageing is very important in cultural heritage applications, as aesthetic changes can be a reason for rejecting the coating from its application on a real object. All coupons were photographed before and after ageing under the same lighting conditions and some differences were visible. Most noticeable is the yellowing of the uncoated brass coupons (Fig. 1a.2) due to the thin oxidation layer formed as reported in the previous work [1]. No large-scale corrosion is visible on any of the coupons, however on steel OW coupons, the electrolyte contact mark is visible where the EIS measurements have been taken (Fig. 1b.1), while on brass it is hardly distinguishable (Fig. 1b.2). It is likely that some of the electrolyte has been retained in the coating and contributed to the oxidation of the steel, which is more sensitive to moisture than brass. On all the B72/TiO$_2$ coupons, waves in the coating are associated to a slight whitening (Fig. 1c). The C80 coupons show differences between the two metals. At t=1 the coating on steel is rough with small pores and white clusters that are visible to the naked eye (Fig. 1d) while on brass it looks fairly uniform. The INC, B72 and PHS/PEOX coatings are apparently unchanged (Fig. 1e.1−3).

Colour measurements
Colour changes after ageing are presented in Table 3. The differences in the L* coordinates show darkening of all the brass coupons, probably due to the formation of

Molina *et al. Heritage Science* (2023) 11:208

Page 5 of 15
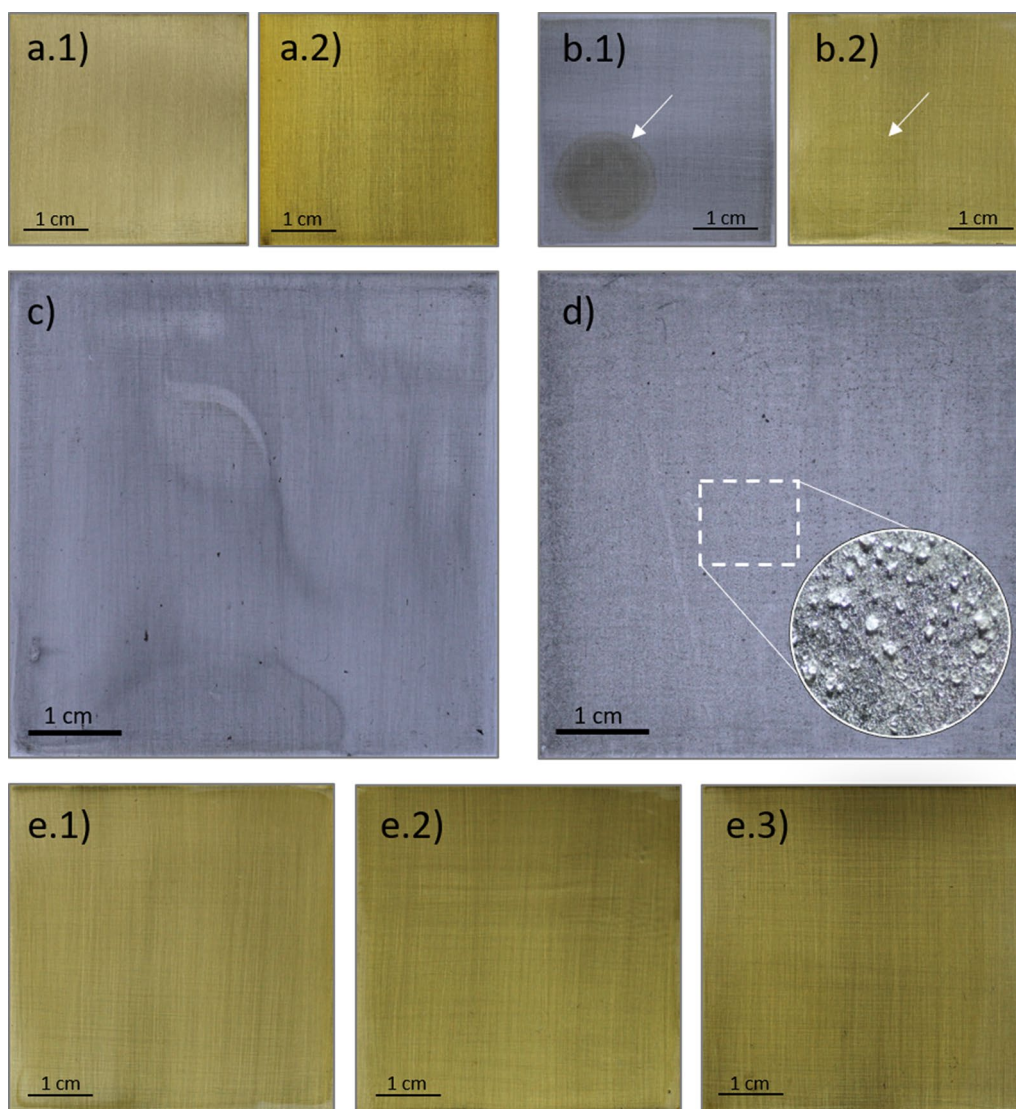
Fig. 1 Macro-pictures of bare brass at t=0 (**a.1**) vs t=1, where its yellowing can be appreciated (**a.2**). EIS measurement mark on Owatrol at t=1 on steel (**b.1**) and on brass (**b.2**). Defects on the coatings of B72/TiO$_2$ on steel before ageing (**c**). Macro+zoom of C80 on steel at t=1 showing the rough surface due to the presence of wax flakes (**d**). The rest of the coatings (**e.1**) PHS/PEOX, (**e.2**) INC and (**e.3**) B72, are apparently unchanged at t=1; only a general yellowing of the metal is visible, as is the uncoated brass

oxidation layer described in Sect. "Visual appearance" and more detectable in the bare coupons ($\Delta L^* = -8.23$) than in the coated ones ($\Delta L^* = -2.30/-4.63$). It is noticeable how the application of all coatings also reduced Δb^* compared to the uncoated ones.

The largest colour differences for both metals occur in the b* coordinate related to yellowing. After 500 h of ageing, all the coatings on brass increase their b* coordinate by several units with respect to t=0. Since the coupons are yellow per se, the coordinates are very different with respect to the steel, in addition the yellowing of the substrate by the oxide layer makes the results incomparable. This observation is in agreement with previous studies [1].

On steel (Fig. 2), the highest changes in b* were detected for OW and PHS/PEOX, followed by INC, with $\Delta b^* = 1.54$, 1.73 and 1.22 respectively. Regarding L* coordinate, on B72/TiO$_2$ an increase in whiteness is particularly evident on steel. Despite these colour changes, none of the coatings on steel exceeded by 3 units in ΔE (colour difference detectable by a standard observer [47]).

Molina *et al. Heritage Science* (2023) 11:208

Page 6 of 15

Table 3 Colour variation measurements in CIELAB 1976 colour space induced by accelerated ageing

	ΔL*		Δa*		Δb*		ΔE	
	Steel	Brass	Steel	Brass	Steel	Brass	Steel	Brass
Bare	− 0.41	− 8.23	− 0.13	1.90	− 0.48	12.10	1.13	14.76
OW	− 0.90	− 3.44	0.07	0.40	1.73	1.05	1.99	3.66
PHS/PEOX	− 0.04	− 2.30	− 0.40	0.38	1.54	3.38	1.68	4.16
B72/TiO$_2$	1.50	− 3.30	− 0.04	0.64	− 0.11	2.66	1.80	4.32
B72	− 0.24	− 3.43	− 0.03	0.45	0.49	4.39	0.87	5.61
INC	− 0.46	− 3.33	− 0.02	0.78	1.22	5.06	1.40	6.13
C80	0.54	− 4.63	− 0.01	0.56	0.49	3.01	0.85	5.56

Difference between aged and unaged samples
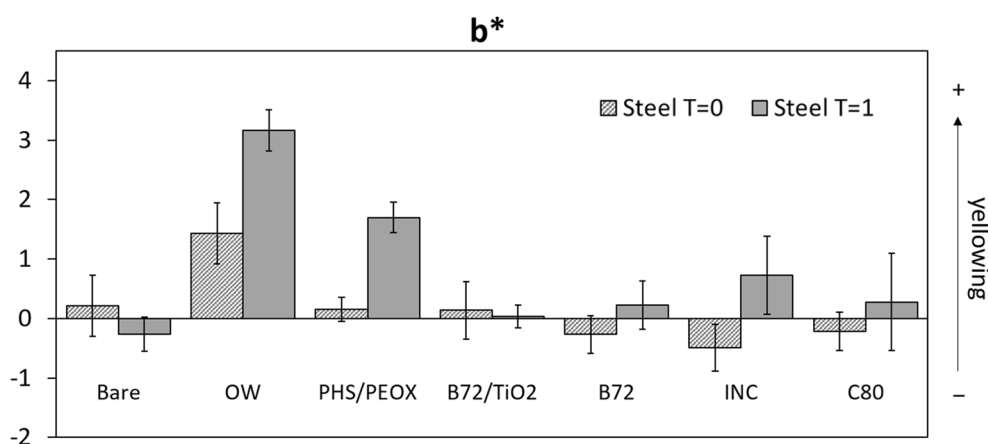
Fig. 2 Differences in b* values between coatings on steel before and after ageing

Protective ability
Thickness measurements

Since the thickness has a great influence on the barrier effect and, consequently, on the protective ability, it has been taken into account to compare the coatings [39]. Thickness measures are listed in Table 4. A significant difference is observed between the coatings that have been diluted before application (B72, B72/TiO$_2$, PHS/PEOX) and those that have been used as prepared by the manufacturer (INC, OW). Indeed, the thickness measurements on the latter coatings are associated to higher standard deviations than those on the former ones. This indicates that the products used as supplied produced quite uneven layers, probably due to higher viscosity and therefore more difficult application without leaving brush strokes. It also shows how the addition of TiO$_2$ to B72 increases the SD by the waves previously seen (Fig. 1c).

After ageing, all the coatings seem to maintain their thickness in the same range with respect to t=0. However, at t=1, a slight generalised decrease in thickness is observed, which may be due to the evaporation of the solvent residues during ageing. B72 and C80 on steel do

Table 4 Thickness values ± SD of the coatings (μm) before and after ageing

	Steel		Brass	
	t=0	t=1	t=0	t=1
OW	29 ± 5	25 ± 5	32 ± 5	30 ± 5
PHS/PEOX	8 ± 2	8 ± 2	10 ± 3	10 ± 3
B72/TiO$_2$	6 ± 3	5 ± 3	10 ± 2	8 ± 2
B72	6 ± 1	7 ± 1	10 ± 2	9 ± 1
INC	27 ± 7	26 ± 6	35 ± 6	34 ± 6
C80	20 ± 5	22 ± 6	21 ± 11	21 ± 9

not follow this trend but fall within the uncertainty values. However, the average decrease in thickness of OW is rather noticeable and occurs on both metals. Taking into account that the curing of alkyd resins such as OW involves not only physical drying but also chemical processes including oxidative crosslinking of the unsaturated fatty acids [48], it is possible that the chemical changes result in significant shrinking of the polymer.

Molina *et al. Heritage Science* (2023) 11:208

Page 7 of 15

Electrochemical impedance

Considering the thicknesses for each of the triplicate coupons and selecting an area with controlled thickness to make the electrochemical measurements before and after ageing for each of them, reproducible results were obtained. EIS data have been represented using Bode plots, which show the logarithm of the impedance modulus, |Z|, and the phase angle, ϕ, versus the logarithm of the frequency. All coupons have been measured except PHS/PEOX because the hydrophilicity of PEOX [23] makes the polymer incompatible with aqueous electrolytes.

After ageing (t = 1), |Z| of all coatings decrease (Figs. 3–4) −with the exception of INC-brass−. OW is the coating with the lowest |Z| at t = 0, despite being one of the thickest. Although defects are not obvious to the naked eye, the coating has not demonstrated much resistance to electrolyte entry at t = 0, and worsens significantly after ageing, since |Z| has decreased almost three orders of magnitude (Fig. 3a). This makes it a poor alternative to common coatings when applied on bare metal and

exposed to solar radiation. Therefore, its performance on patinated or corroded metal needs to be further studied in order to shed light on the contrast between the good results obtained by conservators on real artefacts in terms of appearance and short-term protective ability. [31, 33, 34].

It can be noticed that C80 also presents a significant |Z| decrease upon ageing (Fig. 3b), and a second time constant appears, linked to the formation of defects of the coating (see Sect. "Visualisation of defects") allowing the electrolyte to reach the metal surface. These defects may have been generated by exposing the wax to the test temperature, which may have contributed to a change in its crystalline structure, turning it more amorphous and thus leading to a decrease in resistance [49]. This behaviour is different in the two metals, since on steel |Z| the decrease is not so abrupt and new time constant is more evident. As will be seen in Sect. "Visualisation of defects", the morphological defects are also different in the two metals.
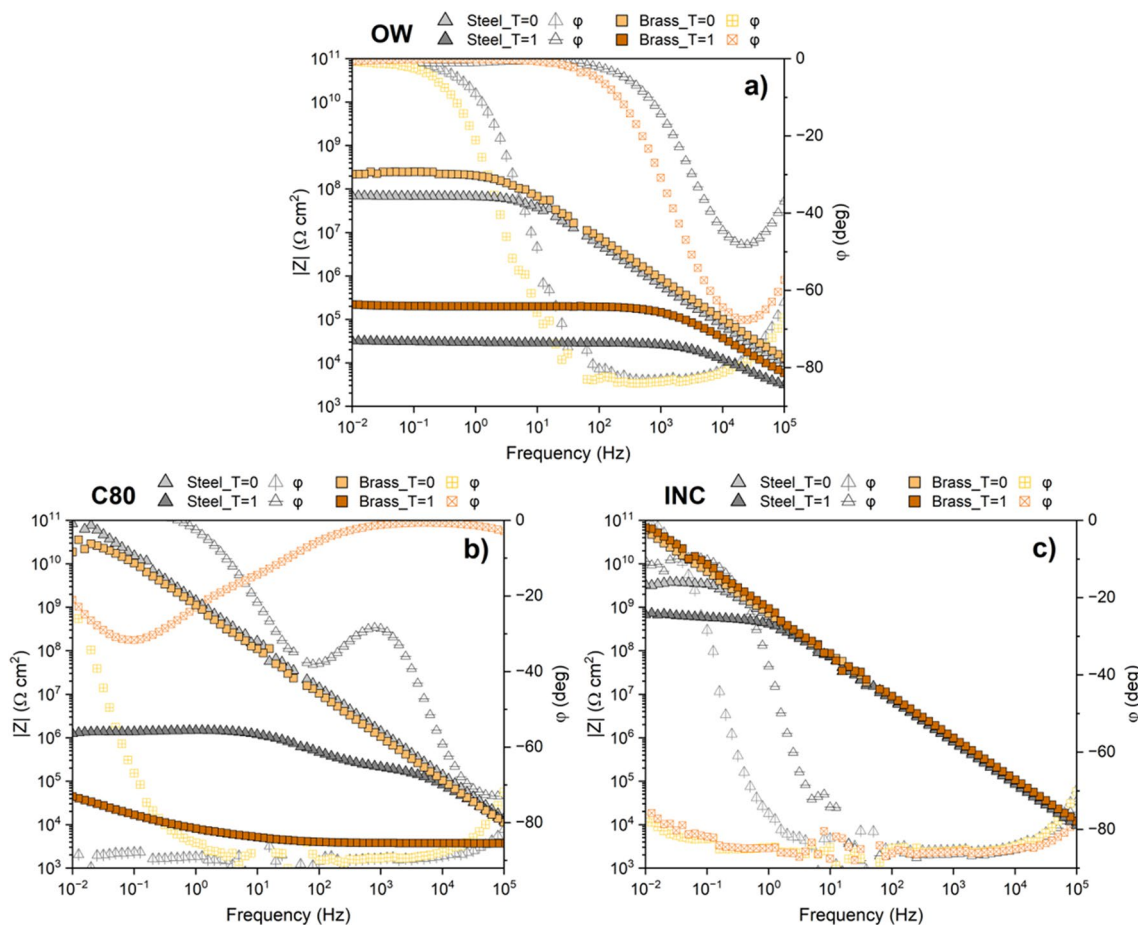
Fig. 3 Comparison of the impedance spectra of OW before and after ageing (**a**) with the spectra of C80 (**b**) and INC (**c**)

Molina *et al. Heritage Science* (2023) 11:208

Page 8 of 15
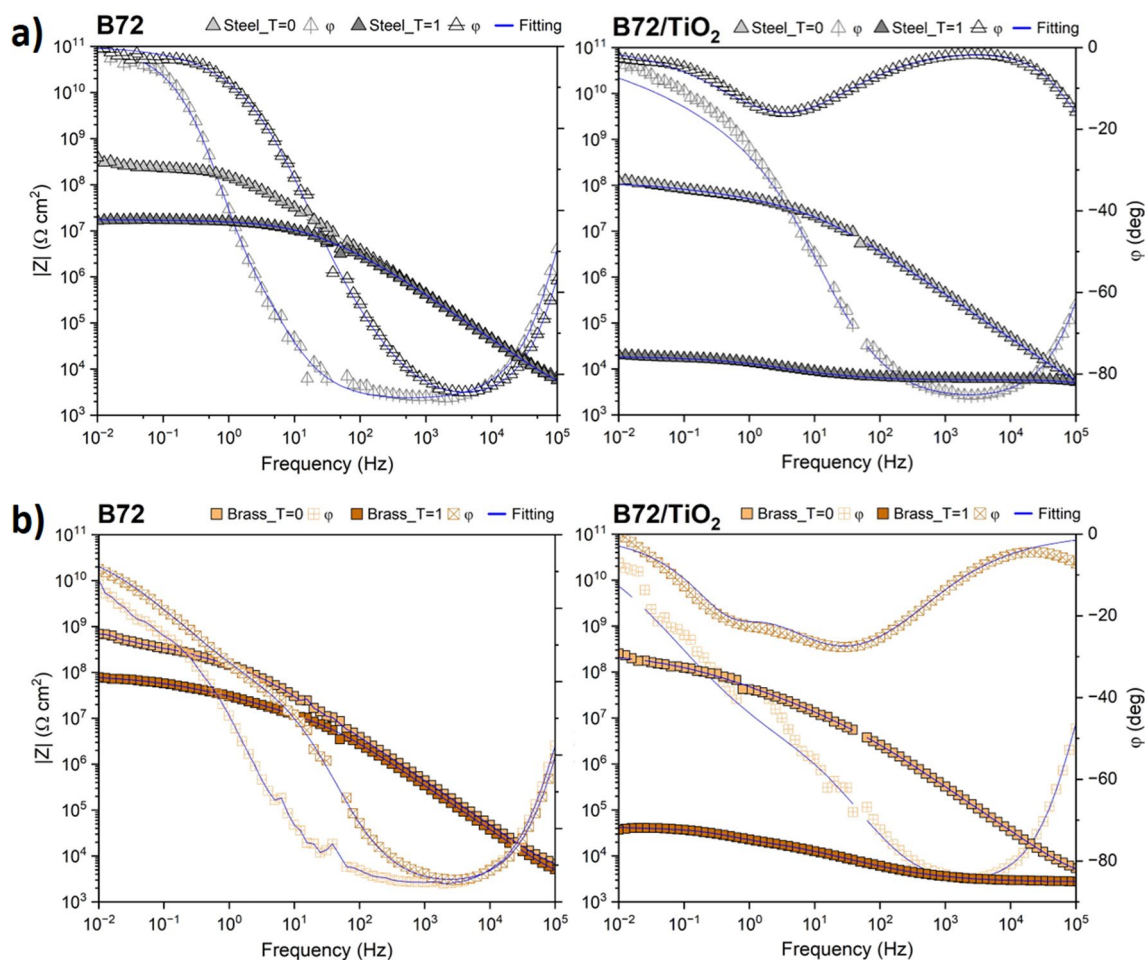
Fig. 4 Comparison of the protective ability of B72 and with the addition of TiO2 NPs before and after accelerated ageing. Impedance spectra and their fitting to EEC of the coatings applied on steel (**a**) and brass (**b**) are plotted

On the other hand, INC continues showing good protective ability after accelerated ageing, as shown in previous studies [37, 50] since |Z| and φ between t = 0 and t = 1 remain almost equal (Fig. 3c). Its good performance is related to the additives, including BTA as corrosion inhibitor and UV stabiliser [38]. The lower thickness of the coating on steel makes clearly visible in |Z| the plateau at the low frequencies, attributable to the resistive behaviour of the coating, and its decrease of about one order of magnitude in |Z| upon ageing. On the other side, on the thicker coating on brass, this plateau appears at frequencies below the experimental limit of the impedance spectrum, making difficult to observe the changes upon ageing.

The effect of TiO_2 nanoparticles on the protective ability of B72 has been represented in Fig. 4 for both steel and brass substrates. At t = 0, it is observed that the addition of NPs slightly lowers the |Z| of the coating on both metals, but their presence does not greatly affect the

protective ability of the coating. However, at t = 1, |Z| decreases by four orders of magnitude and with it the phase angle, where new time constants start to become evident (Fig. 4a, b right). In order to characterise these changes in the spectra, a fitting of the spectra to the equivalent electrical circuit (EEC) shown in Fig. 5 has been carried out. The fitting results are plotted in Fig. 5 over the experimental data, and the parameters of the different elements used presented in Table 5.

All spectra can be fitted to the typical EEC of a coated metal [51] (Fig. 5), in which Rs corresponds to the uncompensated resistance (mainly the electrolyte resistance); CPE_{coat} in parallel to a R_{coat} are attributable to the capacitance of the coating and the resistance of the electrolyte permeating the coating through pores, cracks or paths between the polymeric chains; (CPE_{dl}) is capacitance of the electrochemical double layer and (R_{ct}) the charge transfer resistance of the faradaic process. CPE are usually employed instead of capacitors to account for

Molina *et al. Heritage Science* (2023) 11:208

Page 9 of 15
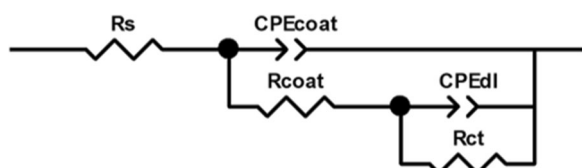
Fig. 5 Equivalent electrical circuit used to fit the experimental data of Fig. 4

the non-ideal behaviour of the electrochemical system. In our case, values of the exponent of the CPE_{coat} very close to 1 indicate an almost ideal capacitive behaviour of the coating, which is lost for B72-TiO_2 after ageing, falling to about 0.5. Values of 0.5, also seen in the exponent of CPE_{dl}, can be attributed to a diffusion process or to a high dispersion of time constants caused by the inhomogeneity of the degraded coating/corrosion products/metal system.

At t = 0, the values of R_{coat} decrease in one order of magnitude for both steel and brass with the addition of TiO_2, indicating that NPs favour the formation of defects in the coating, and hence facilitate the permeation of the electrolyte. For the TiO_2-modified coatings, ageing results in drastic changes. The pore resistance falls rapidly, twice the orders of magnitude than in the B72 coating. Double layer capacitance also shows a significant increase with ageing for B72/TiO_2 coating on both metals, together with a drastic decrease of R_{ct}. This can be related to the increase of the exposed metal surface to the electrolyte, through the high number of pores.

Visualisation of defects

For B72/TiO_2, the hypothesis of increase in surface area exposed to the electrolyte was confirmed by the

microscopic visualisation of the coatings. Figure 6a–c show that the modification of B72 with NPs leads to an increase in porosity and defects (Fig. 6b), particularly pronounced at t = 1 (Fig. 6c). Regarding the visualisation of the other coatings, the presence of scattered pores in OW on both metals (Fig. 6d; steel) and the differences between the defects in the C80 coupons are also confirmed. In brass (Fig. 6e), the restructuring of C80 due to the high temperature of the weathering test has left areas of the metal unprotected, responsible of the decrease in the protective ability. However, in steel (Fig. 6f), this coating looks more compact, with pores instead of gaps, and it accumulates in the form of flakes on the surface. No defects were seen in the INC and PHS/PEOX coatings, so they are not included in the figure.

For a better visualization of the defects formed in B72/TiO_2 on steel and brass and the arrangement of the nanoparticles in the coating, coupons have been observed by electron microscopy. As can be seen in Fig. 7a, on brass at t = 0, most of the NPs are integrated in the coating with hardly any visible defects, while at t = 1 the defects are quite noticeable, creating pores that reveal the metal and TiO_2 (Fig. 7b). The larger pores coincide with clusters of NPs and can be seen to be responsible for the physical deterioration of the polymer (Fig. 7c). This degradation can be related to the generation of high energy free radicals such as O_2^- and OH^- during the photocatalytic process, which are breaking down the polymer matrix [52].

### Evaluation of chemical changes
TR-FTIR measurements

Coatings were characterised before and after ageing with FTIR in reflection mode to determine their chemical stability. The chemical changes occurring to B72-steel can be observed in Fig. 8a. At t = 1, the evident broadening of the carbonyl ester band at 1745 cm^{-1} can be related

Table 5 Electrochemical parameters of the fit of B72 and B72/TiO_2 coatings before and after ageing

Steel	Rs (Ω cm^2)	CPE_{coat}-Y_1 (S s$^{\alpha 1}$ cm^{-2})	α_1	R_{coat} (Ω cm^2)	CPE_{dl}-Y_2 (S s$^{\alpha 2}$ cm^{-2})	α_2	R_{ct} (Ω cm^2)
B72 (t = 0)	3.79E+03	5.70E-10	0.96	1.08E+08	1.29E-09	0.84	1.14E+08
B72 (t = 1)	2.92E+03	4.85E-10	0.97	3.49E+06	4.89E-09	0.59	1.39E+07
B72-TiO_2 (t = 0)	2.37E+03	5.21E-10	0.96	1.04E+07	7.48E-09	0.39	1.22E+08
B72-TiO_2 (t = 1)	2.49E+03	5.14E-10	0.96	3.21E+03	2.34E-05	0.58	1.29E+04
Brass	Rs (Ω cm^2)	CPE_{coat}-Y_1 (S s$^{\alpha 1}$ cm^{-2})	α_1	R_{coat} (Ω cm^2)	CPE_{dl}-Y_2 (S s$^{\alpha 2}$ cm^{-2})	α_2	R_{ct} (Ω cm^2)
B72 (t = 0)	3.82E+03	5.08E-10	0.96	6.12E+07	2.76E-09	0.42	9.29E+08
B72 (t = 1)	2.68E+03	6.41E-10	0.96	6.99E+06	1.16E-08	0.50	8.32E+07
B72-TiO_2 (t = 0)	3.42E+03	6.78E-10	0.96	6.32E+06	6.44E-09	0.53	2.55E+08
B72-TiO_2 (t = 1)	2.71E+03	7.28E-06	0.54	2.68E+04	2.50E-05	0.96	1.36E+04
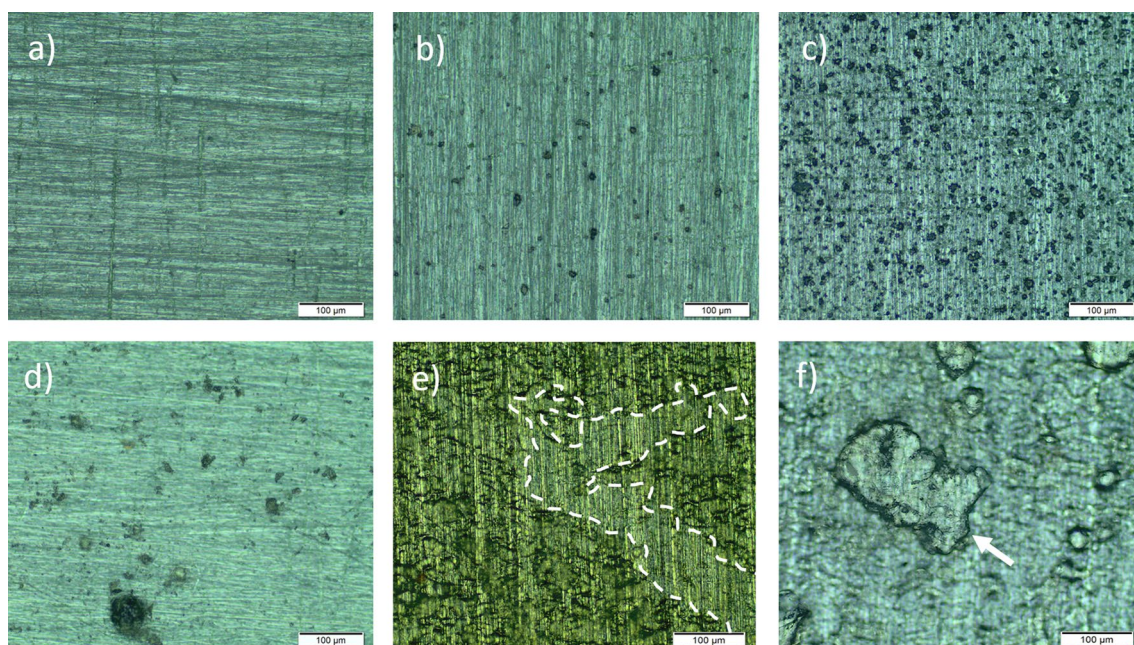
Fig. 6 Comparison of coating defects under microscope. (**a**) B72 on steel at t = 1. No defects are visible. (**b**) B72/TiO$_2$ on steel at t = 0. Addition of NPs leads to the appearance of localised pores. (**c**) B72/TiO$_2$ on steel at t = 1. The appearance of pores grows abruptly. (**d**) Defects of OW on steel at t = 1. (**e**) C80 on brass at t = 1. Wax seems to restructure leaving gaps, with areas of the metal left unprotected (delimited by dashed white line). (**f**) C80 on steel at t = 1. Wax grains (one of these is indicated by the arrow) predominate over a coating with few pores
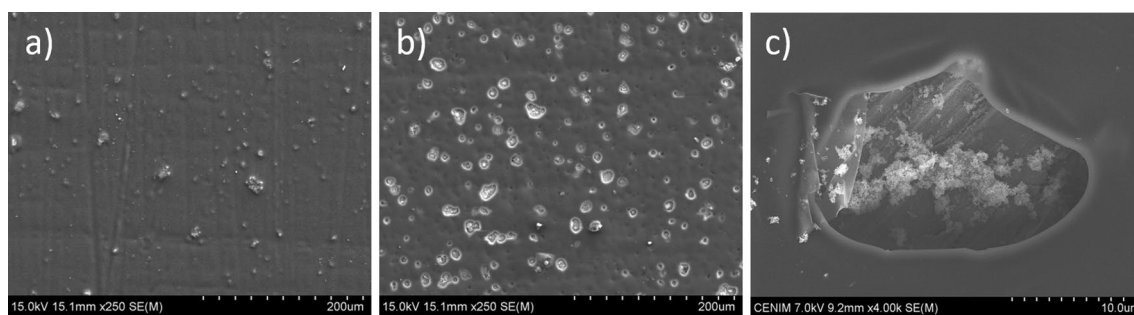

Fig. 7 SEM topographic images of TiO$_2$-modified B72 on brass. (**a**) At t = 0. (**b**) At t = 1 and (**c**) Detail of a pore/defect formed at t = 1, showing the coating, the NPs clusters and the metal

to the evolution of carboxylic acids to anhydrides, either by inter- or intramolecular elimination of water, while the development of the small band at 1640 cm^{-1} can be attributed to the formation of C=C chain-end double bonds [53]. The same applies to brass. Nevertheless, when the polymer is charged with TiO$_2$ NPs, no evident changes to the spectral profile are visible on both metals, suggesting that no significant chemical alterations occur in the bulk of the polymer, as a result of the UV-absorbing action exerted by this additive. At the same time, TiO$_2$ is responsible for the formation of defects in the coating, as previously shown (Fig. 6b, c) and (Fig. 7b, c), which lower its protective ability shown in EIS (Fig. 4).

Thus, it is demonstrated that with the accelerated ageing conditions used, the degradation of B72/TiO$_2$ occurs on a physical scale and its photocatalytic process does not affect chemically the stability of the bulk of the polymer. On the other hand, INC has demonstrated on both metals better chemical stability than B72 without NPs, since only the development of a small band at 1640 cm^{-1} has been observed (Fig. 8b), probably due to the presence of BTA in its composition which also acts as a UV absorber [38, 54].

In OW on both metals (Fig. 8c; brass), the occurrence of chemical changes due to accelerated photo-ageing is suggested by the depletion of methylene vibrations at

Molina *et al. Heritage Science* (2023) 11:208

Page 11 of 15
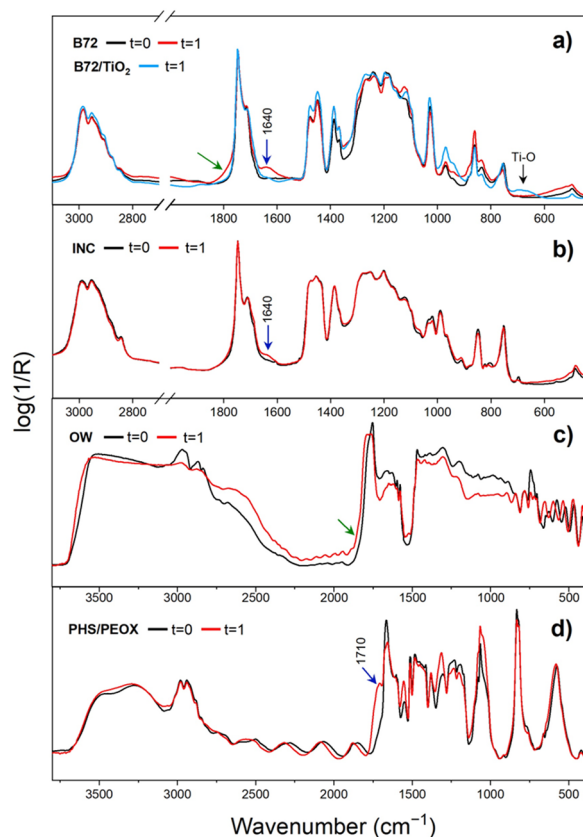
Fig. 8 FTIR evaluation of coatings after accelerated ageing. **a** Represents B72 and TiO₂ spectra on steel, **b** INC spectra on steel. **c** OW spectra on brass and **d** PHS/PEOX spectra on steel. The green arrows show peak broadening, the blue arrows show new peaks and the black arrows show the characteristic peak of the Ti–O-Ti bond
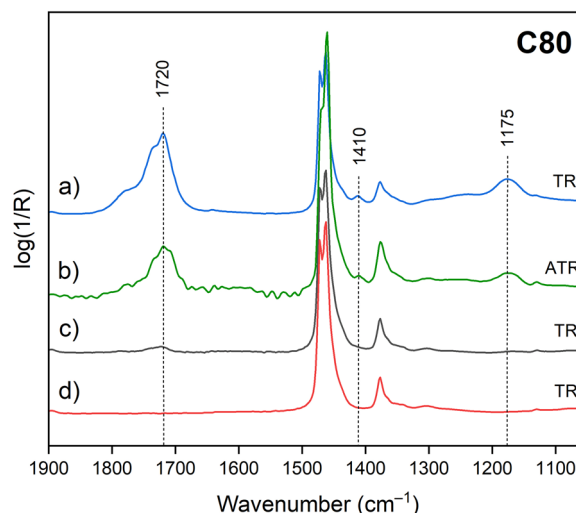
Figure 9 shows the changes that C80 has undergone at t = 1. Spectra on both metals (Fig. 9a, b) reveal new vibration bands at 1720 cm⁻¹, 1410 cm⁻¹ and 1175 cm⁻¹ which can be attributed to C=O stretching, C-H bending and C-O stretching respectively, as a result of oxidation processes and chain rearrangement. These data are in agreement with those obtained in [49] on Butcher's wax (a mixture of carnauba wax and microcrystalline wax), also suggesting that C80 consists of a mixture of different waxes. On C80-brass, these bands are less intense and more difficult to identify with TR-FTIR (Fig. 9c). This is likely due to the oxide layer formed over the metal, which exhibits dielectric optical properties in this IR region and acts as a semiconductor decreasing the absorption [59]. Such hypothesis has been confirmed by performing ATR-FTIR on the coating without the metallic substrate (Fig. 9b).

Comparing FTIR results for C80 for brass and steel with those reported in the previous sections, it can be argued that the cross-linking of the polymer may be more significant on steel than on brass, forming a more insoluble coating that is consistent with the observation of a more compact (Fig. 6) and higher impedance (Fig. 3b), and therefore more protective layer at t = 1.

Evaluation of self-healing ability of PHS/PEOX
Addition of CaCl2
In non-heritage related fields of study, the advantages of coordination bonds in the construction of self-healing polymers have been explored [60]. Metal–ligand coordination bonds are a type of non-covalent interactions that form between a metal ion and the surrounding

2930 and 2850 cm⁻¹, by the increased intensity of the band at ca. 2650 cm⁻¹, attributable to hydroxyls bonded -OH with carboxylic groups, and by the broadening of C=O carbonyl absorption at 1745 cm⁻¹ [55], with appearance of a weak shoulder at 1780 cm⁻¹ which earlier studies related to the formation of either γ-lactones or peresters [56]. These changes suggest oxidation and partial decomposition of the tridimensional network of the molecules, which is in agreement with the decrease in impedance reported in Sect. "Electrochemical impedance". In the 800–400 cm⁻¹ region, interference fringes from the transmitted radiation are visible [57]. With regard to PHS/PEOX, at t = 1 it was observed the appearance of a new band at 1710 cm⁻¹ in the C=O stretching range and some intensity changes in the C-O stretching region (1320–1025 cm⁻¹) (Fig. 8d; steel), which may be attributed to hydrolysis of the ester linkage with formation of free carboxylic groups, as reported in the literature [58]. Interference fringes are also visible between 2600 and 1800 cm⁻¹.

Fig. 9 Comparison of the absorbance of C80 coatings applied on steel (**a**) and brass (**b**, **c**) after ageing. A spectrum on steel at t = 0 is added as a reference (**d**)

Molina *et al. Heritage Science* (2023) 11:208

Page 12 of 15

organic molecules. In the case of PHS/PEOX synthesis, the addition of the CaCl$_2$ salt accelerates the self-healing efficiency by a ternary bonding effect and increases the adhesion strength in both wet and ambient environments [22]. In heritage conservation, the use of soluble salts is not recommended because they can degrade the material, and in our case corrode the metal. However, for this work, some steel and brass coupons were prepared with a low proportion of CaCl$_2$ to test if an improvement of the self-repairing ability could be achieved without any damage or aesthetic changes in the metal. But after 48 h of drying corrosion of the metal substrate was already observed (Fig. 10). Although corrosion was only visible in small proportion on brass, the application of soluble salts was discarded in both cases and no further testing was carried out.

Procedure and damage regeneration
To evaluate the self-healing efficiency of the polymer, a set of steel and brass coupons that was not exposed to accelerated ageing was prepared. After application and drying of the coating, a series of mechanical damages were performed with a scalpel. The width of the scratches ranged from 50 to 400 µm. In some regions the incision left the metal exposed, while in others the damage was more superficial.
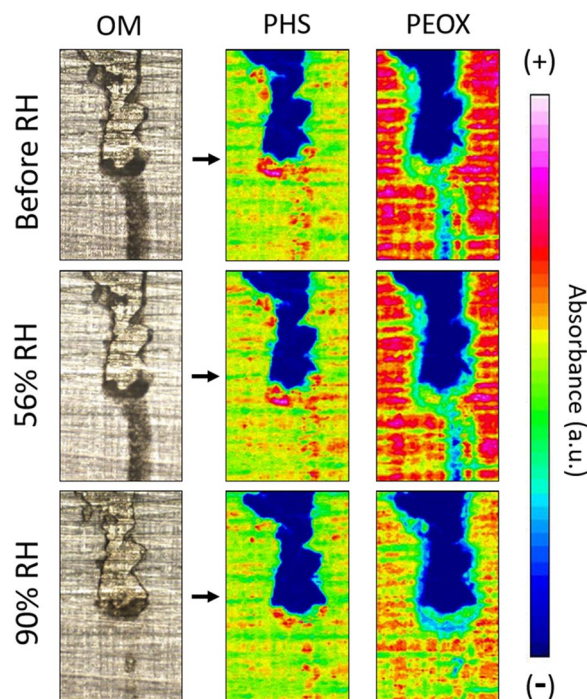
Considering the sensitivity of our substrates to humidity, the coatings were first subjected to a relative humidity of 54% at 35 ℃ for 3 h in a climatic chamber. Under these conditions, half of the damage of approximately 50–100 µm was regenerated in the reference study on glass [22]. On steel and brass this is not the case and the scratches remained the same size. However, when the same coupons were subjected to 90% relative humidity at 35 ℃ for another 3 h, changes were visible (Fig. 11; OM images) and the more superficial and narrower scratches were almost completely regenerated.

The spatial distribution of PHS/PEOX components in the coating was monitored with chemical imaging using FPA-FTIR. The most characteristic peaks, the C=O stretching band at 1660 cm^{-1} and the semicircle stretching modes of the benzene at 1515 cm^{-1}, were selected for PEOX and PHS respectively. As shown in Fig. 11, PEOX initially exhibits high intensity on the surface where there is no scratch due to its higher proportion in the polymer, while PHS reflects how the area with the highest intensity corresponds to the accumulation of polymer. After 90% RH, the decrease in PEOX intensity combined with the disappearance of the most superficial part of the scratch suggests the redistribution of the polymer over the coupon surface. A certain redistribution of PHS is also observed, so that both components of the polymer have shown mobility and a fairly homogeneous spatial distribution after exposure to humid environments.

The behaviour of the polymer on steel is similar, even though less pronounced. Figure 12a shows a deep scratch in the coating. While no evident changes were observed after exposure to low humidity, it seems that polymer redistribution occurred at high humidity, as visible at the microscope (Fig. 12b). As shown by chemical imaging (Fig. 12c), the intensities of PHS and PEOX bands slightly increase in the upper part of the scratch, suggesting that these two components of the polymer moved. However,

Fig. 10 Macro-photos of PHS/PEOX + CaCl$_2$ on steel (left) and on brass (right) after 48 h of drying. Corrosion is observed to be higher in the areas where more coating accumulated after application

Fig. 11 Regeneration monitoring with OM and FPA-FTIR, of a scratch made on PHS/PEOX-brass before and after being subjected to 56% RH and 90% RH. The absorbance of the most characteristic peak of PHS and PEOX is represented

Molina *et al. Heritage Science* (2023) 11:208

Page 13 of 15

corrosion of the substrate started to develop locally (Fig. 12b).

These preliminary results show that an optimisation of the conditions used is required to obtain a good self-healing ability of the coating and to increase the viability of use in metallic heritage. PHS/PEOX has shown acceptable behaviour after ageing, with no aesthetic or morphological changes observed. However, the high humidity required to achieve redistribution of the polymer is the limiting factor because it promotes corrosion of the metal, so further research is needed in this area.

Conclusions

In this work, new alternatives for the protection of bare brass and steel surfaces in metal artefacts have been explored and compared to other more traditional coatings. On both steel and brass, Owatrol demonstrated poor protective properties and significant chemical changes upon ageing, which are related to a tendency to yellowing. The performance of the C80 wax has been better in its initial state. After ageing, it has lost almost all its protective ability due to the defects formed by its restructuring during the ageing test. In addition, it has presented a high photo-oxidation that has formed an insoluble deposit on the steel, which could affect its reversibility.

Our results have shown that charging Paraloid B-72 with TiO_2 nanoparticles reduces the oxidation suffered by the polymer upon UV photo-ageing. However, it also increases degradation on a physical scale with massive pore opening and hence dramatically worsens the protective ability of the coating. The presence of these morphological defects would leave the metal of the artefact more exposed to humidity − or rain in an outdoor environment − and would cause its corrosion, so its use is not recommended. In these environments, Incralac is the best alternative among all the coatings studied, as it has obtained the best performance in all the parameters tested.

PHS/PEOX has demonstrated good performance after accelerated ageing, as no morphological defects have been identified and no aesthetic changes have been obtained. Its use would be limited only to artefacts exposed indoors, as rain could dissolve the coating.
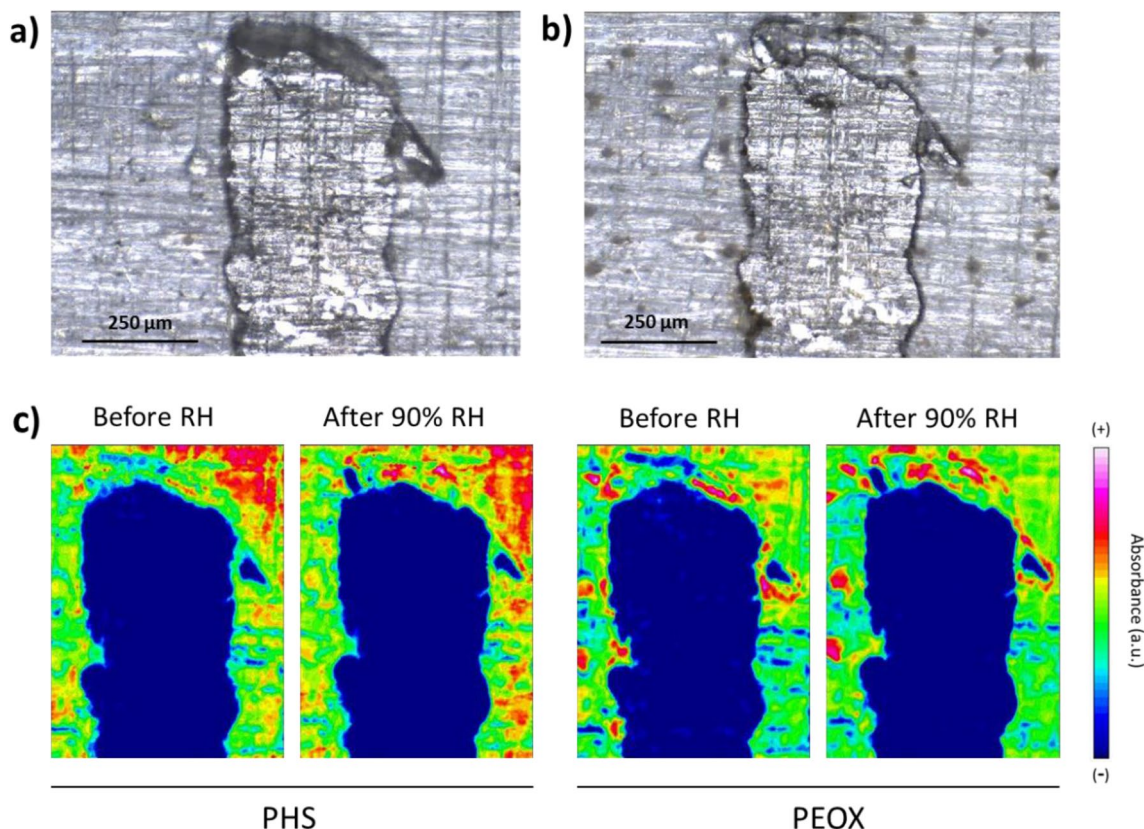
Fig. 12 Differences between the PHS/PEOX coating on steel seen under the optical microscope. **a** Scratch of the coating before exposure to humidity in the climatic chamber and **b** Steel corrosion, after exposing the coating to 90% RH and 35 ℃ for 3 h. **c** Chemical distribution map of the two polymer components before and after exposure to relative humidity. The same scale in absorbance as in Fig. 10 is followed

Molina *et al. Heritage Science* (2023) 11:208

Page 14 of 15

Self-healing properties at low and high humidity have been explored and it has been shown that the polymer has only redistributed when exposed to 90% RH and 35 ℃ for 3 h. Under these conditions, only the most superficial and narrowest areas of the previously made scratches were sealed.

These conditions, especially the humidity, are too high for metal artefacts on display in a museum; however, the results obtained in this work are very relevant, as the first ones on the application of this type of coatings for protection of metallic heritage. If a compromise can be found between low relative humidity and longer exposure time during the regeneration process, this coating would be a viable protective coating in some cases, such as regenerating surface damages on the protective coating suffered during the operation of some scientific-technical artefacts. Before they can be actually applied for conservation treatments, further research is required, including aspects such as its performance on surfaces with different degrees of corrosion, ageing under different environmental conditions (indoor/outdoor), reversibility, performance on different metals, and limited testing on actual artefacts.

Author contributions
MTM: methodology, data curation, formal analysis, investigation and writing—original draft. BS: formal analysis, investigation, resources, validation, visualization and writing—review & editing. EC: funding acquisition, project administration, resources, visualization, supervision and writing—review & editing. DDF: funding acquisition, conceptualization, visualization and writing—review & editing. BRB: conceptualization, methodology, supervision, validation, visualization, writing—review & editing.

Availability of data and materials
The datasets generated and analysed during the current study will be available in the following institutional repository: https://digital.csic.es/.

Declarations

Ethics approval and consent to participate
Not applicable.

Consent for publication
Not applicable.

Competing interests
The authors declare that they have not competing interests.

References

1. Molina MT, Cano E, Leal J, Fort R, Álvarez de Buergo M, Ramírez-Barat B. Protective coatings for metals in scientific-technical heritage: the collection of the spanish national museum of science and technology (MUNCYT). Heritage. 2023;6:2473–88.
2. Chiantore O, Trossarelli L, Lazzari M. Photooxidative degradation of acrylic and methacrylic polymers. Polymer. 2000;41:1657–68.
3. Zhuang S, Lv X, Pan L, Lu L, Ge Z, Wang J, et al. Benzotriazole UV 328 and UV-P showed distinct antiandrogenic activity upon human CYP3A4-mediated biotransformation. Environ Pollut. 2017;220:616–24.
4. Molina MT, Cano E, Ramírez-Barat B. Protective coatings for metallic heritage conservation: a review. J Cult Herit. 2023;62:99–113.
5. Mihelčič M, Slemenik Perše L, Šest E, Jerman I, Giuliani C, Di Carlo G, et al. Development of solvent- and water-borne fluoropolymer protective coatings for patina-free bronze discs. Prog Org Coatings. 2018;125:266–78.
6. Kosec T, Škrlep L, Švara Fabjan E, Sever Škapin A, Masi G, Bernardi E, et al. Development of multi-component fluoropolymer based coating on simulated outdoor patina on quaternary bronze. Prog Org Coatings. 2019;131:27–35.
7. Kiele E, Lukseniene J, Griguceviciene A, Selskis A, Senvaitiene J, Ramanauskas R, et al. Methyl-modified hybrid organic-inorganic coatings for the conservation of copper. J Cult Herit. 2014;15:242–9.
8. Zucchi F. Sol-gel coatings for the preservation of metallic heritage artefacts. In: Dillmann P, Watkinson D, Angelini E, Adriaens A, editors. Corros conserv cult herit met artefacts. Cambridge: Woodhead Publishing; 2013. p. 540–51.
9. Wang D, Bierwagen GP. Sol-gel coatings on metals for corrosion protection. Prog Org Coatings. 2009;64:327–38.
10. Montemor MF. Functional and smart coatings for corrosion protection: a review of recent advances. Surf Coatings Technol. 2014;258:17–37.
11. Burgos-Cara A, Rodríguez-Navarro C, Ortega-Huertas M, Ruiz-Agudo E. Bioinspired alkoxysilane conservation treatments for building materials based on amorphous calcium carbonate and oxalate nanoparticles. ACS Appl Nano Mater. 2019;2:4954–67.
12. Speziale A, González-Sánchez JF, Taşcı B, Pastor A, Sánchez L, Fernández-Acevedo C, et al. Development of multifunctional coatings for protecting stones and lime mortars of the architectural heritage. Int J Archit Herit. 2020;14:1008–29.
13. Lettieri M, Colangiuli D, Masieri M, Calia A. Field performances of nano-sized TiO2 coated limestone for a self-cleaning building surface in an urban environment. Build Environ. 2019;147:506–16.
14. Chiavari C, Balbo A, Bernardi E, Martini C, Zanotto F, Vassura I, et al. Organosilane coatings applied on bronze: influence of UV radiation and thermal cycles on the protectiveness. Prog Org Coatings. 2015;82:91–100.
15. Monticelli C, Zanotto F, Grassi V, Seyedi M, Balbo A. Improving the protectiveness of 3-mercaptopropyl-trimethoxysilane coatings on bronze by addition of oxidic nano-andmicroparticles. Coatings. 2020;10:225.
16. Wang J, Wu Y, Zhang S. A new coating system modified with nano-sized particles for archaeological bronze protection. Stud Conserv. 2014;59:268–75.
17. Mokhtarifar M, Kaveh R, Bagherzadeh M, Lucotti A, Pedeferri MP, Diamanti MV. Heterostructured TiO2/SiO2/γ-Fe2O3/rGO coating with highly efficient visible-light-induced self-cleaning properties for metallic artifacts. ACS Appl Mater Interfaces. 2020;12:29671–83.
18. Chen XD, Wang Z, Liao ZF, Mai YL, Zhang MQ. Roles of anatase and rutile TiO2 nanoparticles in photooxidation of polyurethane. Polym Test. 2007;26:202–8.
19. Scalarone D, Lazzari M, Chiantore O. Acrylic protective coatings modified with titanium dioxide nanoparticles: comparative study of stability under irradiation. Polym Degrad Stab. 2012;97:2136–42.

Molina *et al. Heritage Science* (2023) 11:208

Page 15 of 15

20. Giuntoli G, Bini M, Ciuffi B, Salvadori B, Baldi G, Rosi L. Nanodispersions of TiO2 in water for removing acrylic films used in conservation. Polymers. 2021;13:3966.

21. Stankiewicz A, Szczygieł I, Szczygieł B. Self-healing coatings in anti-corrosion applications. J Mater Sci. 2013;48:8041–51.

22. Zhang Y, Zhang K, Li X, Li T, Ye Q, Tan LL, et al. Self-healable transparent polymer/salt hybrid adhesive via a ternary bonding effect. J Mater Chem A. 2020;8:21812–23.

23. Zhang Y, Li X, Wei B. Environment-friendly poly(2-ethyl-2-oxazoline) as an innovative consolidant for ancient wall paintings. Nanomaterials. 2018;8:649.

24. La Nasa J, Di Marco F, Bernazzani L, Duce C, Spepi A, Ubaldi V, et al. Aquazol as a binder for retouching paints. an evaluation through analytical pyrolysis and thermal analysis. Polym Degrad Stab. 2017;144:508–19.

25. Molina MT, Cano E, Llorente I, Ramírez-Barat B. Corrosion risk to metal-based artefacts in a scientific and technical museum: an assessment of environmental and exhibition conditions. Materials. 2023;16:4239.

26. Prytulak G. CCI Note 9/8: Mechanical removal of rust from machined ferrous surfaces. Ottawa; 1996.

27. Prytulak G. CCI Note 15/4: Indoor display of industrial collections. Ottawa; 1998.

28. Lanterna G, Giatti A. Caratterizzazione non invasiva delle vernici da ottone degli strumenti scientifici: ricette storiche, realizzazione di provini verniciati, ricerca analitica e applicazioni "in situ" su strumenti storici. OPD Restauro Riv dell'Opificio delle pietre dure e Lab di restauro di Firenze. 2014;26:165–80.

29. Newey H. Conservation and the preservation of scientific and industrial collections. Stud Conserv. 2000;45:137–9.

30. Brunott M, Greiner A, Hallam D, Thurrowgood D. Conservation maintenance programs for functional objects. In: Mardikian P, Chemello C, Watters C, Hull P, editors. METAL 2010, Proc Interim Meet ICOM-CC MWG 11–15 October, 2010. Charleston, South Carolina: ICOM-CC; 2010. p. 421–9.

31. Mardikian P. Epave du CSS Alabama—conservation du canon RML Blakely. 2020. https://hal.archives-ouvertes.fr/hal-02495211v2/. Accessed 3 Apr 2023.

32. Farrell E, K. McGath M, Echerd J. Testing the compressive strength and reversibility of consolidants applied to marine archaeological gray cast iron. In: Mardikian P, Näsänen L, Arponen A, (eds). Met 2022 Proc Interim Meet ICOM-CC Met Work Group Helsinki: Helsinki; 2022. p. 114–22.

33. Boellinghaus T, Wentland E, Jassmann R, Keller R, Wolfrum A. Conservation of the shaft #1 headgear at the Tsumeb mine, Namibia: corrosion protection. Stud Conserv. 2021;68:228–42.

34. Mazzon C, Letardi P, Braggerhoff S. Development of monitoring techniques for coatings applied to industrial heritage. In: TICCIH members (eds) Big Stuff Heritage 2015 Conference: Lewarde, France; 2015.

35. Ramírez-Barat B, Cano E. In situ assessment of protective coatings for metallic cultural heritage using electrochemical impedance spectroscopy. Ge-Conservacion. 2015;8:6–13.

36. Wolfe J, Grayburn R, Khanjian H, Heginbotham A, Phenix A. Deconstructing Incralac: A formulation study of acrylic coatings for the protection of outdoor bronze sculpture. In: Brigland J (eds). ICOM-CC 18th Trienn Conf: Copenhagen; 2017.

37. Masi G, Josse C, Esvan J, Chiavari C, Bernardi E, Martini C, et al. Evaluation of the protectiveness of an organosilane coating on patinated Cu-Si-Mn bronze for contemporary art. Prog Org Coatings. 2019;127:286–99.

38. Wolfe J, Grayburn R. A review of the development and testing of incralac lacquer. J Am Inst Conserv. 2017;56:225–44.

39. Molina MT, Cano E, Ramírez-Barat B. Testing protective coatings for metal conservation: the influence of the application method. Herit Sci. 2023;11:1–9.

40. ISO 16474-2:2014. Paints and varnishes—methods of exposure to laboratory light sources. Part 2: xenon arc lamps. 2014.

41. Banerjee S, Pillai SC, Falaras P, O'shea KE, Byrne JA, Dionysiou DD. New insights into the mechanism of visible light photocatalysis. J Phys Chem Lett. 2014;5:2543–54.

42. UNE-EN 15886:2010. Conservation of cultural property—test methods—Colour measurement of surfaces. 2010.

43. Ramírez Barat B, Cano E, Letardi P. Advances in the design of a gel-cell electrochemical sensor for corrosion measurements on metallic cultural heritage. Sens Actuators B Chem. 2018;261:572–80.

44. Cano E, Crespo A, Lafuente D, Ramirez BB. A novel gel polymer electrolyte cell for in-situ application of corrosion electrochemical techniques. Electrochem Commun. 2014;41:16–9.

45. Tetreault J. Airborne pollutants in museums, galleries and archives : risk assessment, control strategies and preservation management. Ottawa: Canadian Conservation Institute; 2003.

46. Ramírez Barat B, Cano E. Agar versus agarose gelled electrolyte for in situ corrosion studies on metallic cultural heritage. ChemElectroChem. 2019;6:2553–9.

47. Mokrzycki W, Tatol M. Color difference Delta E-A survey. Mach Graph Vis. 2011;20:383–411.

48. Muizebelt WJ, Nielen MWF. Oxidative crosslinking of unsaturated fatty acids studied with mass spectrometry. J Mass Spectrom. 1996;31:545–54.

49. Swartz N, Clare TL. On the protective nature of wax coatings for culturally significant outdoor metalworks: microstructural flaws, oxidative changes, and barrier properties. J Am Inst Conserv. 2015;54:181–201.

50. Ellingson LA, Brostoff LB, Shedlosky TJ, Bierwagen GP, De la Rie ER. The use of electrochemical impedance spectroscopy in the evaluation of coatings for outdoor bronze. Stud Conserv. 2004;49:53–62.

51. Ramírez Barat B, Cano E. In situ electrochemical impedance spectroscopy measurements and their interpretation for the diagnostic of metallic cultural heritage: a review. ChemElectroChem d; 2018; 2698–716.

52. Li W, Lin J, Zhao Y, Pan Z. The adverse effects of TiO2 photocatalycity on paraloid B72 hybrid stone relics protective coating aging behaviors under UV irradiation. Polymers. 2021;13:262.

53. Chiantore O, Lazzari M. Photo-oxidative stability of paraloid acrylic protective polymers. Polymer. 2001;42:17–27.

54. Giuntoli G, Rosi L, Frediani M, Sacchi B, Salvadori B, Porcinai S, et al. Novel coatings from renewable resources for the protection of bronzes. Prog Org Coatings. 2014;77:892–903.

55. Lazzari M, Chiantore O. Drying and oxidative degradation of linseed oil. Polym Degrad Stab. 1999;65:303–13.

56. Mallégol J, Gardette J, Lemaire J. Long-term behavior of oil-based varnishes and paints photo and thermooxidation of cured linseed oil. J Am Oil Chem Soc. 2000;77:257–63.

57. Derrick MR, Stulik D, Landry JM. Infrared spectroscopy in conservation science scientific tools for conservation. Los Angeles: The Getty Conservation Institute; 1999.

58. Agarwal M, Koelling KW, Chalmers JJ. Characterization of the degradation of polylactic acid polymer in a solid substrate environment. Biotechnol Prog. 1998;14:517–26.

59. Bermudez VM. Infrared optical properties of dielectric/metal layer structures of relevance to reflection absorption spectroscopy. J Vac Sci Technol A Vacuum, Surfaces, Film. 1992;10:152–7.

60. Li CH, Zuo JL. Self-healing polymers based on coordination bonds. Adv Mater. 2020;32:1903762.

Publisher's Note